MoSe$_2$ in flower spheres provides abundant active sites for TiO$_2$ photocatalytic degradation of RhB

M. Xie[a], W.W. Lu[a], W. Yan[a], Y. C. Wei[a], Y. P. Chen[ab], J. Xu[ab*]
[a]School of Physics and Electronic Engineering, Jiangsu University, Zhenjiang, Jiangsu, 212013, P. R. China
[b]Quantum Sensing and Agricultural Intelligence Detection Engineering Center of Jiangsu Province, Zhenjiang, Jiangsu, 212013, P. R. China

In this paper, a MoSe$_2$/TiO$_2$ composite photocatalyst was constructed by modifying TiO$_2$ with MoSe$_2$ as a group catalyst. The results showed that pure TiO$_2$ and MoSe$_2$ had no degradation activity for RhB, and the composite catalyst of 0.03 g MoSe$_2$ had the best photocatalytic degradation activity for RhB. Through SEM, TEM, UV-VIS absorption spectrum, transient photocurrent curve, photoluminescence spectrum, and electrochemical impedance spectrum analysis, it can be seen that the excellent performance of 0.03 g MoSe$_2$ composite sample is due to its excellent nanostructure, and uniform TiO$_2$ nanosheets are attached to MoSe$_2$ flower spheres. The active site of RhB photocatalytic degradation was increased, the visible light response and photobiological carrier separation were enhanced, and TiO$_2$ had photocatalytic activity under simulated sunlight.

1. Introduction

In recent years, with the development of industry and technology, China's national economy has leaped forward in development, but at the same time, China's ecological environment has been seriously damaged because of various industrial pollution [1-2]. Among all kinds of environmental pollution, water pollution and air pollution, which have attracted much attention, have caused serious threats to people's lives and health to a large extent [3-5]. In particular, the water pollution caused by organic matter which is highly toxic, difficult to degrade, and has "three effects" not only causes harm to the natural environment but also seriously affects the survival of human beings [6-7]. Therefore, in recent years, water purification has become one of the hot spots of scientific workers, and to solve this problem, researchers have proposed a variety of organic pollution water treatment methods, such as the chemical oxidation method, physical adsorption method, and microbial degradation method. Photocatalytic oxidation technology for wastewater treatment has been an effective environmental protection technology for water treatment in the past 30 years [8]. The key to the application of this technology is the selection and application of

---

photocatalysts [9]. At present, most N-type semiconductor materials are used as catalysts for heterogeneous photocatalytic degradation of organic pollutants in water bodies [10]. In recent years, the semiconductor materials used for research and development are mainly metal oxides or sulfides, such as TiO_2, SnO_2, WO_3, V_2O_5, CdS, etc [11-14]. Among them, TiO_2 is recognized as an environmentally friendly photocatalytic material with the most potential for development and application in the field of environmental pollution control due to its good photo corrosion resistance and catalytic activity, stable physical and chemical properties, non-toxic and harmless, cheap and easy to obtain [15].

However, for a single TiO_2 nanomaterial, the electron-hole pair generated under the irradiation of a certain frequency light source is prone to bulk phase or surface composite, thereby reducing the photocatalytic performance of titanium dioxide, and TiO_2 only absorbs ultraviolet light of a certain frequency, which greatly limits the practical application of TiO_2 [16]. Therefore, how to realize the solar efficiency of titanium dioxide and improving its photocatalytic ability has been the goal of the majority of scholars. At present, effective methods used to improve TiO_2 photocatalytic activity include metal ion doping, nonmetallic element doping, precious metal deposition, binary composite semiconductor method, etc., among which, binary composite semiconductor method is an effective means to improve TiO_2 photocatalytic efficiency [17-19]. The photocatalyst formed by a simple combination or doping of two semiconductors or a semiconductor and an insulator material becomes a binary composite semiconductor photocatalyst. In the process of forming this photocatalyst, the conduction band and valence band of the two materials that constitute the binary composite semiconductor photocatalyst have different energy levels of photogenerated electrons, and holes may be separated through transportation, which will reduce their recombination probability and thus improve the photocatalytic activity of TiO_2 [20]. This method of composite semiconductor material or insulator material onto TiO_2 has become a method recommended by many scholars and experts in recent years. Many studies have been conducted in this regard. For example, semiconductors that compound with TiO_2 to form binary composite in-vivo photocatalysts include ZnO, Fe_2O_3, SnO_2, Al_2O_3, WO_3, In_2O_3 and CdS [21-22]. $MoSe_2$, composed of the basic crystal unit Se-Mo-Se, is a narrow-band layered semiconductor material. Photoelectron spectroscopy analysis shows that the energy band of $MoSe_2$ ($\approx 1.4eV$) can match the sunlight spectrum well. It has also been reported that the transition of photons in $MoSe_2$ is between the non-bonded metal d state, which makes $MoSe_2$ have good photo corrosion resistance [23]. These excellent properties make $MoSe_2$ potentially valuable in the field of photocatalysis.

In this work, we first synthesized $MoSe_2$ flowers and then synthesized $MoSe_2/TiO_2$ composite photocatalyst by hydrothermal coupling with TiO_2. $MoSe_2/TiO_2$ catalysts exhibit stronger visible light response and more efficient carrier separation. The degradation rate of $MoSe_2/TiO_2$ heterojunction is better than that of $MoSe_2$ and TiO_2. This is thanks to the rounded structure of $MoSe_2$ flowers.

2. Experimental section

2.1. Chemicals

Sodium molybdate ($Na_2MoO_4 \cdot 2H_2O$), analytically pure; Selenium powder, analytically pure; Sodium borohydride ($NaBH_4$), analytically pure; Sodium hydroxide ($NaOH$), analytically pure; Ammonia fluotitanate (($NH_4)_2TiF_6$), analytically pure; Anhydrous ethanol (C_2H_6O), pure analysis, the above drugs are Sinopharm Group Chemical reagent Co., LTD products.

2.2. Preparation of MoSe$_2$ nanomaterials

Use a measuring cylinder to measure 25 mL of distilled water and pour it into a beaker. Use a balance to weigh 1.6452 g $Na_2MoO_4 \cdot 2H_2O$, 1.5492 g Se powder, and 0.2595 g $NaBH_4$, respectively, and add them into the beaker containing distilled water successively under magnetic stirring. Stir until evenly dispersed. Add 25 mL anhydrous ethanol into a beaker with a measuring cylinder, stir for 5 min, transfer the blood red mixture to a 100 mL high-temperature hydrothermal reactor and seal it, put the reactor into a vacuum drying oven, and keep it warm at 200 $^{\circ}$C for 6 h. After the oven is cooled to room temperature naturally, the upper red liquid is poured out, the black product is collected, and the black powder is obtained after drying with distilled water and anhydrous ethanol. 50 mL 0.2 mol/L NaOH solution was prepared, and the black powder was added to the NaOH solution under magnetic stirring. After stirring evenly, the black powder was sealed with plastic wrap and kept in an oven at 80 $^{\circ}$C for 2 h to remove the remaining Se in the reactants. After natural cooling to room temperature, filtered, washed, and dried, MoSe$_2$ was obtained.

2.3. MoSe$_2$/TiO$_2$ nanocomposites were prepared

Weigh 3.0 g ($NH_4)_2TiF_6$ and add it into a book containing 50 mL distilled water under magnetic stirring. After the crystal is completely melted, weigh a certain amount of MoSe$_2$ prepared in step 1 and add it into the above solution, stir well, and then ultrasonic treatment for 5 min. The mixture was then transferred to a 100 mL high-temperature hydrothermal reactor lined with polytetrafluoroethylene and sealed, and the reactor was placed in a vacuum drying oven and kept at 180 $^{\circ}$C for 12 h. After natural cooling to room temperature, after washing and drying, MoSe$_2$/TiO$_2$ nanocomposites were obtained.

3. Photocatalytic performance test

The visible-light catalytic activity of MoSe$_2$/TiO$_2$ nanocomposites was evaluated by the photodegradation rate of Rhodamine B solution under simulated sunlight degradation.

Take 50 mL of Rhodamine B solution with a certain concentration and put it into a 100 mL bethel, add 50 mg of the prepared MoSe$_2$/TiO$_2$ nanocomposite material into it, and disperse it evenly by ultrasound. Then transfer the solution to the flat-bottom flask of the GHX-2 photochemical reaction meter, and fix the flask. The solution was stirred magnetically for 30 min under the condition of avoiding light and open air. When the adsorption-desorption equilibrium was reached, 4 mL of the solution was extracted and placed in the centrifuge tube, and then the light was turned on. Samples were taken when the reaction time was 5 min, 15 min, 25 min, 55 min, 85 min, 115 min, 145 min, 175 min, 205 min, and 240 min, and about 4 mL of solution were

taken, numbered successively, and stored away from light. After that, the solutions obtained at different photolysis reaction times were centrifuged. The absorbance of the supernatant obtained by centrifugation was determined by UV-2550 UV-visible spectrophotometer at 500 nm.

$$\Phi = (A_0 - A) / A_0 \times 100\%$$

A_0: indicates the absorbance of the solution without reaction;

A: indicates the absorbance of the solution at a certain point in the reaction.

The degradation rate Φ of Rhodamine B solution at any photolytic reaction time can be calculated.

4. Characterization

The phase analysis of the obtained samples was carried out by a German D8ADVANCE X-ray diffractometer (Cu Kα1 ray, λ=0.15418 nm). The micromorphology of the samples was observed by emission scanning electron microscope (FESEM, JEOL JSM-7001F) and transmission electron microscope (TEM, JEM-100CXII). A solid diffuse reflection UV-Vis absorption spectrometer (UV-VIS) was used to analyze the absorption of the samples in UV-visible light. The absorbance of the Rhodamine B solution in the photocatalytic reaction was determined by UV-2550 UV-visible spectrophotometer.

5. Results and discussion

The X-ray diffraction spectra of $MoSe_2/TiO_2$ nanocomposites obtained by adding different $MoSe_2$ after calcination at 450 $^{\circ}$C and Ar gas protection for 1 h are shown in Fig. 1. As can be seen from Fig. 1a, when 0.03 g $MoSe_2$ is added, the diffraction peaks of the products belong to the as TiO_2 [20], and only two diffraction peaks (002) and (100) appear at 13.58° and 33.74°, which are the characteristic peaks of $MoSe_2$ [22]. This indicates that the prepared product is $MoSe_2/TiO_2$ composite material. As the amount of $MoSe_2$ continues to increase (0.15 g Fig. 1b and 0.21 g Fig. 1c), the diffraction peak of TiO_2 in the XRD pattern will gradually weaken, and some characteristic peaks will disappear, while the diffraction peak of $MoSe_2$ will gradually increase, and other characteristic peaks will gradually appear, which indicates that $MoSe_2$ and TiO_2 have a good composite.
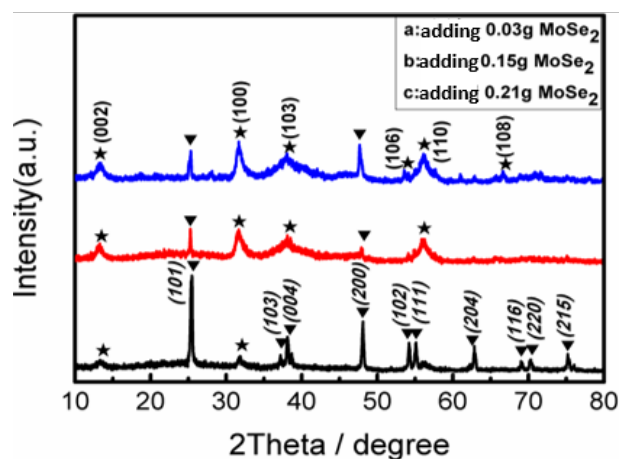
Fig. 1. XRD pattern of the as-obtained composite with different MoSe2 contains a) adding 0.03 g MoSe2;
b) adding 0.15 g MoSe2; c) adding 0.21 g MoSe2.

As shown in Fig. 2, SEM and TEM can clearly and intuitively demonstrate the morphology and microstructure of the obtained samples. Fig. 2a-c shows the SEM images of the products under different magnifications when 0.03 g $MoSe_2$ is added. The low-power scan (Fig. 2a) shows that the sample is composed of uniformly distributed and uniformly sized TiO_2 sheets, and only a small amount of flower-like structures appear in the circled parts of the figure, which may be caused by the small amount of $MoSe_2$ added.
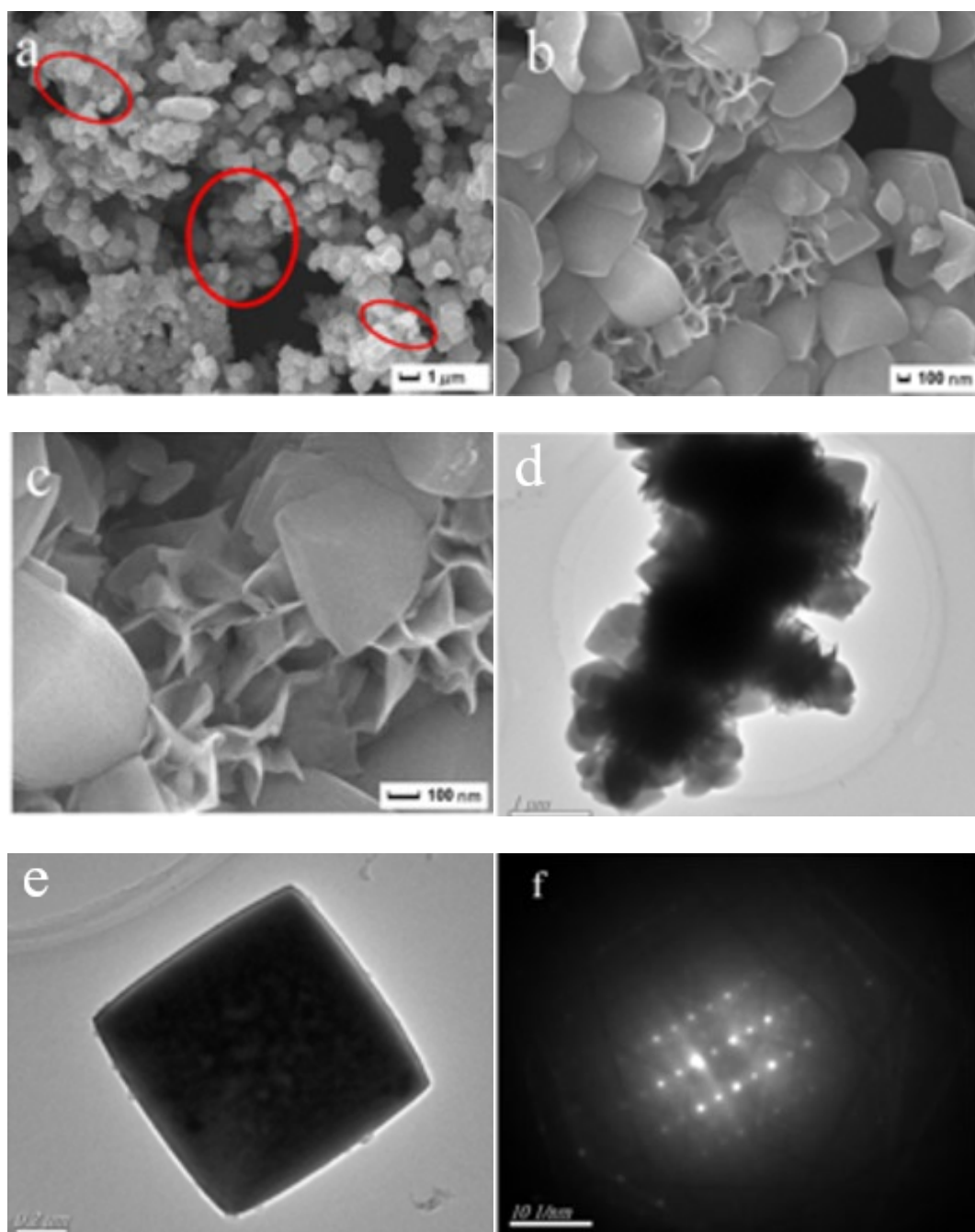
Fig. 2. SEM and TEM images of the as-obtained composite with 0.03 g MoSe2 added.

It can be seen from the enlarged SEM (Fig. 2b) that the product is composed of a polygonal sheet structure with a diameter of about 1 μm and many nanosheets with a thickness of several nanometers. These nanosheets fold and cross each other and are wrapped by the polygonal sheet structure. From the high-power SEM (Fig. 2c), it can be seen that the polygonal TiO_2 sheet has a smooth surface and a thickness of about 100 nm. Fig. 2d-f is the TEM diagram of the product. It can be seen from the figure that the composite material is mainly composed of a extraneous sheet structure and a flower-like structure composed of nanosheets. The extraneous sheet structure

is anatase TiO_2, and the flower-like structure composed of nanosheets is $MoSe_2$. After 30 min of ultrasonic dispersion, the morphology of the composite can still be maintained, which proves that the composite has a relatively stable structure. Fig. 2e is the TEM image of a single TiO_2 tetragonal slice. From the contrast degree of light and shade of the tetragonal slice, we can see that the tetragonal slice has a solid structure and relatively thick thickness. The Fourier transform image of its HRTEM (Fig. 2f) is composed of some well-arranged diffraction spots, which proves that the generated TiO_2 has a single crystal structure.

To study the light absorption properties of the prepared composite materials, Uv-Vis was used to characterize the products prepared when different $MoSe_2$ was added, and the results were shown in Fig. 3. It can be seen from the figure that the optical absorption band edge of pure phase TiO_2 is about 380 nm wavelength, and there is strong absorption in the ultraviolet region (200 nm~380 nm), which is due to the excited transition of O 2p orbital electrons to Ti 3d orbit. As can be seen from Fig. 3b-d, the products added with $MoSe_2$ not only have strong absorption in the ultraviolet region but also have strong absorption in the visible region (wavelength 400-800 nm). Compared with Fig. 3b-d, it can be seen that in the composite process, the more $MoSe_2$ added, the stronger the absorption of visible light by the product. This phenomenon of absorption in the visible region of $MoSe_2/TiO_2$ nanocomposites may be caused by electron transition from the O 2p orbital to the doped level or from the doped level to the conduction band, or it may be due to the strong interaction between $MoSe_2$ and TiO_2, resulting in the absorption of $MoSe_2/TiO_2$ nanocomposites in the visible region.
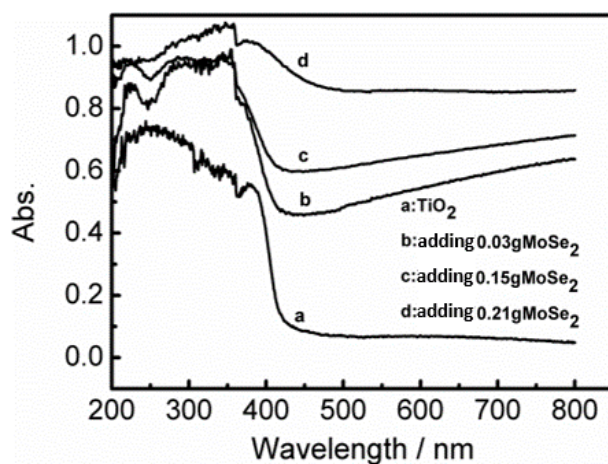
Fig. 3. Uv-Vis diffuse reflection absorption spectra of MoSe2/TiO2 nano-composite: a) pure TiO2; b) adding 0.03 g MoSe2; c) adding 0.15 g MoSe2; d) adding 0.21 g MoSe2.

Fig. 4 shows the change curve of the degradation rate of 50 mL 1.5×10^{-5} mol/L Rhodamine B solution for samples prepared under simulated sunlight with time. As can be seen from the figure, after 30 min of magnetic stirring under air in a dark room, the prepared $MoSe_2/TiO_2$ nanocomposites showed obvious adsorption effect on Rhodamine B, which may be caused by the large specific surface area of the obtained composites. After the light was turned on, pure TiO_2 prepared by the same method had almost no degradation effect on Rhodamine B, and

the degradation rate of Rhodamine B was only 4.6% after 4 h. This is mainly because TiO_2 is a wide-bandgap semiconductor, which hardly absorbs visible light, so it has almost no degradation effect on Rhodamine B. Compared with pure TiO_2, $MoSe_2/TiO_2$ nanocomposites prepared by adding 0.03 g $MoSe_2$ showed obvious visible light catalytic activity, and the degradation rate of Rhodamine B reached 91.3% when the reaction time was 4 h. The addition of $MoSe_2$, a narrow-band gap semiconductor, can improve the absorption of visible light by the composite material, and further promote the photocatalytic activity of TiO_2. Therefore, the $MoSe_2/TiO_2$ nanocomposites prepared by this method are a kind of catalyst with high photocatalytic performance and certain application prospects.
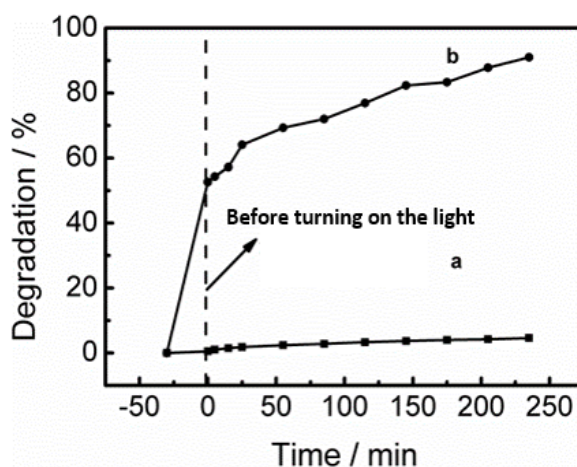
Fig. 4. The photodegradation of RhB aqueous solution for a) pure TiO_2 and b) $MoSe_2/TiO_2$ composite under visible light irradiation.

Fig. 5 shows the absorbance curve of Rhodamine B solution degraded by visible light of $MoSe_2/TiO_2$ nanocomposite prepared by adding 0.03 g $MoSe_2$ with time. As shown in the figure, under visible light irradiation, the characteristic absorption peak of Rhodamine B solution at 554 nm gradually decreased with the extension of time. After 235 min, the characteristic absorption peak of the solution disappeared, indicating that Rhodamine B molecules in the solution were almost completely degraded after 235 min of visible light irradiation. In addition, it can also be seen from the figure that with the extension of time, the absorption peak intensity at 270 nm and 360 nm also gradually decreased, indicating that the intermediate products produced in the degradation process of Rhodamine B were also gradually degraded. It can be seen that the prepared $MoSe_2/TiO_2$ nanocomposites have good visible light catalytic degradation performance of Rhodamine B solution.
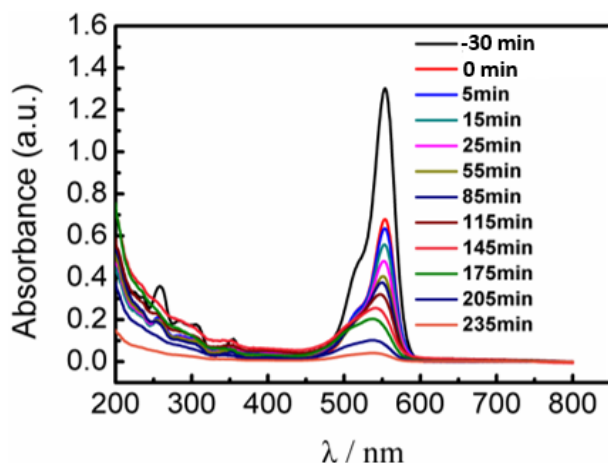
Fig. 5. UV-Vis spectra changes of RhB in aqueous MoSe2/TiO2 dispersions as a function of irradiation time under visible light irradiation.

In addition, under the same conditions, the visible light catalytic activity of the degradation Rhodamine B solution prepared by $MoSe_2/TiO_2$ composite material with 0.15 g and 0.21 g $MoSe_2$ was also tested, and the results showed that for the low concentration of RhB $(1.5 \times 10^{-5}$ mol/L) solution, After stirring in the dark room for 30 min, RhB in the solution was absorbed completely, as shown in Fig. 6. To this end, we further increased the concentration of RhB solution to 3.0×10^{-5} mol/L and conducted experiments. The results are shown in Fig. 6, and the degradation trend was similar to Fig. 5. Based on the above analysis, it can be seen that with the increase of $MoSe_2$ addition, the adsorption effect of $MoSe_2/TiO_2$ composite on RhB solution increases. Due to the strong adsorption effect, the effect of $MoSe_2$ addition on the visible light catalytic performance of the composite remains to be further studied.
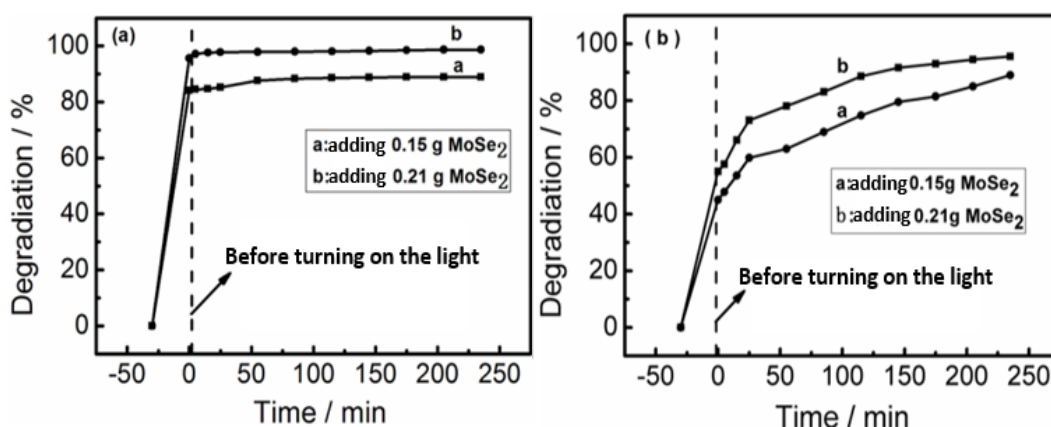
Fig. 6. The photodegradation of RhB aqueous solution for a) 50 mL 1.5×10-5 mol/L RhB and b) 50 mL 3.0×10-5 mol/L RhB under visible light irradiation.

6. Conclusion

In this work, flower-ball $MoSe_2$ was applied to improve TiO_2 activity. The excellent activity of degrading RhB mainly comes from two aspects. The first aspect: as a group of catalysts, flower-ball $MoSe_2$ has a higher specific surface area while providing many active sites to reduce the chemical energy of RhB degradation. The second aspect: the modification of TiO_2 can expand the visible light absorption, so that the composite catalyst can produce more photogenerated electrons than the single catalyst. In addition, this work inspires the exploratory research on improving the optical absorption of TiO_2.

References

[1] Ajibade, P. A, N. Solomane, B. M. Sikakane, Chalcogenide Letters, 19, 6 (2022); https://doi.org/10.15251/CL.2022.196.429

[2] Bhatkhande, Dhananjay S, Vishwas G. Pangarkar, Anthony A. C. M, Environmental & Clean Technology, 77, 1 (2002); https://doi.org/10.1002/jctb.532

[3] Liang. L, Mo. Z, Li. N, Liu. H, Feng. G, Wei. A, Chalcogenide Letters, 17, 11 (2020); https://doi.org/10.15251/CL.2020.1711.555

[4] Akpan, Uduak G, Bassim H. Hameed, Journal of hazardous materials, 170, 2-3 (2009); https://doi.org/10.1016/j.jhazmat.2009.05.039

[5] A. Houas, H. Lachheb, M. Ksibi, E. Elaloui, C. Guillard, J. M. Herrmann, Applied Catalysis B: Environmental, 31, 2 (2001).

[6] Tanaka, Keiichi, Kanjana Padermpole, Teruaki Hisanaga, Water research, 34, 1 (2000); https://doi.org/10.1016/S0043-1354(99)00093-7

[7] Akbal, Feryal, A. Nur. Onar, Environmental monitoring and assessment, 83, (2003); https://doi.org/10.1023/A:1022666322436

[8] Bandala. E. R, Glover. S, Leal. M. T, Arancibia-Bulnes. C, Jimenez. A, Estrada. C. A, Catalysis Today, 76, 2-4 (2002); https://doi.org/10.1016/S0920-5861(02)00218-3

[9] Jing. H. P, Wang. C. C, Zhang. Y. W, Wang. P, Li. R, RSC Advances, 4, 97 (2014); https://doi.org/10.1039/C4RA08820D

[10] Wen. X. J, Niu. C. G, Zhang. L, Liang. C, Guo. H, Zeng. G. M, Journal of catalysis, 358, (2018); https://doi.org/10.1016/j.jcat.2017.11.029

[11] Chen. X, Wu. Z, Liu. D, Gao. Z, Nanoscale research letters, 12, 1-10 (2017); https://doi.org/10.1186/s11671-017-1904-4

[12] Yasmina. M, Mourad. K, Mohammed. S. H, Khaoula. C, Energy Procedia, 50, (2014); https://doi.org/10.1016/j.egypro.2014.06.068

[13] Deng. P. K, Xu. Y. Y, Xu. J, Wang. L. L, Li. D. S, Liu. Q. Q, Research on Chemical Intermediates, 48, (2022); https://doi.org/10.1007/s11164-022-04749-y

[14] Zhang. H, Tang. G. G, Wan. X, Xu. J, Tang. H, Applied Surface Science, 530, (2020); https://doi.org/10.1016/j.apsusc.2020.147264

[15] Akpan. Uduak G, Bassim H. Hameed, Journal of hazardous materials, 170, 2-3 (2009); https://doi.org/10.1016/j.jhazmat.2009.05.039

[16] Dong. H, Zeng. G, Tang. L, Fan. C, Zhang. C, He. X, He. Y, Water Research, 79, (2015); https://doi.org/10.1016/j.watres.2015.04.038

[17] Mahmoodi, Niyaz Mohammad, Journal of Colloid and Interface Science, 295, 1 (2006); https://doi.org/10.1016/j.jcis.2005.08.007

[18] Reza, Khan Mamun, A. S. W. Kurny, Fahmida Gulshan, Applied Water Science, 7 (2017)

[19] Lakshmi. S, R. Renganathan, S. Fujita, Journal of Photochemistry and Photobiology A: Chemistry, 88, 2-3 (1995); https://doi.org/10.1016/1010-6030(94)04030-6

[20] Zheng. S, Yong. C, Kevin E. O'Shea, Journal of Photochemistry and Photobiology A: Chemistry, 210, 1 (2010); https://doi.org/10.1016/j.jphotochem.2009.12.004

[21] Hu. X, Peng. Q, Zhou. L, Tan. X, Jiang. L, Ning. Z, Chemical Engineering Journal, 380, (2020); https://doi.org/10.1016/j.cej.2019.122366

[22] Chiou. C. H, Wu. C. Y, Juang. R. S, Chemical Engineering Journal, 139, 2 (2008); https://doi.org/10.1016/j.cej.2007.08.002

[23] Tang. G. G, Chen. W. T, Wan. X, Zhang. F. X, Xu. J, Colloids and Surfaces A, 587, 2019; https://doi.org/10.1016/j.colsurfa.2019.124291